Available online at www.sciencedirect.com
SCIENCE DIRECT®
ELSEVIER
Engineering Structures 25 (2003) 729–742
ENGINEERING STRUCTURES
www.elsevier.com/locate/engstruct

Thermo-mechanic model for concrete exposed to elevated temperatures

B.M. Luccioni [ab,*], M.I. Figueroa [b], R.F. Danesi [ab,1]

[a] *CONICET, Argentina*
[b] *Structures Institute, National University of Tucumán, Av. Roca 1800, S.M. de Tucumán, Argentina*

Received 14 October 2002; received in revised form 20 November 2002; accepted 1 December 2002

Abstract

A thermo-mechanical model for concrete subjected to high temperatures is presented in this paper. The model is based on a coupled plastic-damage model that has been extended to consider damage induced by high temperatures. The model is calibrated with experimental results of residual strength tests in concrete specimens.

The paper is completed with application examples and comparisons with experimental results that validate the model presented. The model is also used to the damage assessment of a concrete structure that has been subjected to fire.

Keywords: Concrete; Temperature; Damage; Plasticity; Thermal damage; Thermo-mechanical coupling; Numerical model

1. Introduction

In many modern engineering problems concrete results exposed to temperature ranges over ambient conditions (higher than 50°C), as when it takes part of industrial installations (pressure furnaces, chimneys, nuclear reactors), or in accidental situations like explosions or fire.

High temperatures induce severe micro-structural changes that alter mechanical properties of Portland cement concrete [1,2]. The pore structure and thought its physical properties change with time following the hydration and aging processes and they are strongly influenced not only by the mechanical load but also by the thermal-hygrometric state of concrete and their time history.

The physical and chemical changes in concrete under high temperatures depend not only on the matrix composition but also on the type of aggregate (mineralogical characteristics, dilatation [3], etc.). Other factors that have influence are the water/cement ratio, the porosity, humidity and age of concrete [1,4]. As the cement paste is exposed to increasing temperatures the following effects can be distinguished: the expulsion of evaporable water (100°C), the beginning of the dehydratation of the hydrate calcium silicate (180°C), the decomposition of calcium hydroxide (500°C) and of the hydrate calcium silicate (that begins around 700°C). The alterations produced by high temperatures are more evident when the temperature surpasses 500°C. At this temperature level, most changes experienced by concrete can be considered irreversible.

In addition to the temperature levels, the degree of damage depends on the exposition time and the type of cooling experienced by the structural elements. Bibliography is coincident in the fact that most of the alteration is produced in the first two hours of exposure to high temperatures. It is also affirmed that, in general, the strength in tests performed at high temperatures is higher than that obtained for the same specimens previously cooled. The strength loss is greater when the specimens are rapidly cooled. This fact can be attributed to the micro-cracking produced in the material by tension stresses [1,3].

Among the most important effects of high temperatures, the following can be mentioned: dehydratation of cement paste, porosity increase, modification in moist

* Corresponding author. Tel./Fax: +54-381-4364087.
[1] Present address: Muñecas 586, 1° A, 4000 S.M. de Tucumán, Argentina

0141-0296/03/$ - see front matter © 2003 Elsevier Science Ltd. All rights reserved.
doi:10.1016/S0141-0296(02)00209-2

Nomenclature

α	Thermal isotropic dilation coefficient
α_{kl}	Dilatation coefficients tensor
β_{ij}	Thermo-elastic coupling tensor
δ	Vertical displacement
δ_{ij}	Delta de Kronecker symbol
ε_{ij}	Strain tensor
ε^e_{ij}	Elastic strain tensor
ε^p_{ij}	Plastic strain tensor
η	Specific entropy
κ^d	Mechanical damage hardening variable
κ^p	Plastic hardening variable
$\dot{\lambda}$	Plastic consistence parameter
ν	Poisson coefficient affected by the thermal damage process
ν_o	Poisson coefficient at the reference temperature
θ	Measure of temperature
θ_o	Reference temperature
θ_{imp}	Imposed temperature
$\theta^{\max}_{imp}$	Maximum imposed temperature
ρ	Density
σ_{ij}	Stress tensor
ω	Thermal damage variable
Θ	Nodal temperatures vector
Ψ	Free energy density per unit volume
Ψ^e	Thermo-elastic free energy density per unit volume
Ψ^p	Thermo-plastic free energy density per unit volume
Ψ^ω	Thermo-damage free energy density per unit
$\boldsymbol{b}$	Volumetric external forces vector
c_k	Specific heat
d	Mechanical damage variable
$\boldsymbol{f}_\theta$	Thermal forces vector
$\boldsymbol{f}_\omega$	Vector related to the heat loss due to the thermal damage
f_c	Compression strength
f_{co}	Compression strength at the reference temperature
f_{cy}	Compression elastic limit
f^d_{red}	Damage reduction function due to the thermal damage process
f^p_{red}	Plastic reduction function due to the thermal damage process
f_t	Tension strength
f_{to}	Tension strength at the reference temperature
$\boldsymbol{f}^{\mathbf{ext}}_{\mathbf{u}}$	External mechanical forces vector
$\boldsymbol{f}^{\mathbf{int}}_{\mathbf{u}}$	Internal forces vector
h	Conduction convection coefficient
k	Conductivity
l:	Latent heat of thermal damage
p_i	Set of internal plastic variables
$\boldsymbol{q}$	Heat flux vector
q_i	Heat conduction flux
r	Heat sources distributed per unit of volume
t	Time
$\boldsymbol{t}$	External surface forces vector
x_i	Spatial coordinates
$\boldsymbol{B}$	Matrix relating the strains with the nodal displacements
$\boldsymbol{C}_\theta$	Caloric capacity matrix

C^s_{ijkl}	Secant constitutive tensor
E	Elastic modulus affected by the thermal damage process
$E_{\,o}$	Elastic modulus at the reference temperature
G	Plastic potential function
G_f	Fracture energy
$\boldsymbol{K}_\Theta$	Thermal conductivity matrix
K_{ij}	Plastic hardening tensor
$K^d(\kappa^d,\omega)$	Damage hardening function
$K^p(\kappa^p,\omega)$	Function of plastic hardening
$\boldsymbol{M}_u$	Dynamic mass matrix
$\boldsymbol{N}_\theta$	Temperature interpolation functions
$\boldsymbol{N}_\mathbf{u}$	Displacement interpolation functions
P	Load
$\boldsymbol{U}$	Nodal displacements vector

content, thermal expansion, retraction, alteration of pores steam pressure, strength loss, thermal cracking due to thermal incompatibility, thermal creep and thermal spalling due to the excessive pores steam pressure [1,5,6].

At the structural level, the behaviour of concrete elements exposed to high temperatures is characterized by spalling, that is a brittle failure with most cracks parallel to the heated surface.

The behaviour of structures exposed to fire is normally described in terms on their fire resistance, that is the period of time of fire exposure for which failure is attained [7–9].

The prediction of the behaviour under fire is usually made from tests in furnaces of isolated elements. Many experimental works related to the effect of high temperatures in concrete have been published in the last decades [10,11,1,12,13,3,4]. The use of the results of this type of tests for a complete structure implies many simplifying assumptions. The principal differences between these tests and what happens in real structures are due to boundary conditions [8]. A way to solve this problem is to perform tests in complete structures but, in many cases, it can be impracticable. This is the reason for what the interest in analytical or numerical methods for evaluation of fire performance of structures has been increasing in the last decade.

An accurate numerical model for concrete under high temperatures should be able to simultaneously include many non linear effects such as heat conduction, vapour diffusion, liquid water flux due to pressure gradients, capillarity effects and gradients in the adsorbed water content, so as the transfer of latent heat due to the change of phase of the water inside the pores.

Among the more recent works, the thermo-mechanical models presented by Heinfling et al [2], Gawin et al [14], Ju et al [5], Ulm et al [6] may be cited. All these models require complex thermodynamical developments and numerical algorithms appropriate for the treatment of coupled problems.

2. Constitutive model

A coupled plastic damage model [15] extended to take into account the effects of high temperatures in the mechanical behaviour of concrete is presented in this paper. The model is able to reproduce the increment in porosity, the loss of strength, the degradation of the elastic modulus and the variation in Poisson coefficient so as the modification of plastic and damage behaviour due to the exposure to high temperatures. Coupled thermo-mechanical analysis of concrete structures can be performed with this model included in a non-linear thermo-mechanical finite element program.

2.1. Thermodynamic basis

The model is based on the assumption of uncoupled elasticity [16]. According to this hypothesis, the free energy density can be supposed to be formed by two independent parts: a thermo-elastic part and a thermo-plastic part [6]. A third term due to thermal damage is added in this case [19,20],

$$\Psi(\varepsilon^e_{ij},p_i,d,\omega,\theta) = \Psi^e(\varepsilon^e_{ij},d,\omega,\theta) + \Psi^p(p_i,\omega) + \Psi^\omega(\omega,\theta) \quad (1)$$

where Ψ is the free energy density per unit volume, Ψ^e is the thermo-elastic free energy density per unit volume, Ψ^p is the thermo-plastic free energy density per unit volume, Ψ^ω is the thermo-damage free energy density per unit volume, $\varepsilon^e_{ij} = \varepsilon_{ij} - \varepsilon^p_{ij}$ is the elastic strain tensor, ε_{ij} is the strain tensor, ε^p_{ij} is the plastic strain tensor, d is the mechanical damage variable, p_i is a set of internal plastic variables, θ is a measure of temperature, ω is the thermal damage variable that represents a measure of the deterioration produced by high temperatures and is such that,

$$0 \le \omega \le 1 \quad (2)$$

The following expression for the thermo-elastic free

energy density per unit volume, based on that proposed by Stabler [17] for high temperature increments, is used in this paper,

$$\Psi^e = \frac{1}{2}\varepsilon^e_{ij} C^s_{ijkl}(d,\omega)\varepsilon^e_{kl} - (\theta-\theta_o)\beta_{ij}(d,\omega)\varepsilon^e_{ij} + c_\kappa(d,\omega)\left[\theta-\theta_o-\theta\ln\left(\frac{\theta}{\theta_o}\right)\right] \quad (3)$$

where $C^s_{ijkl}(d,\omega) = \dfrac{\partial^2\Psi^e(d,\omega)}{\partial\varepsilon^e_{ij}\partial\varepsilon^e_{kl}}$ is the secant constitutive tensor affected by the mechanical damage and by the process of thermal damage and θ_o is the reference temperature.

The secant damaged stiffness tensor takes into account a scalar mechanical damage and an isotropic thermal damage characterized by a variation in the elastic modulus and the Poisson coefficient as functions of the thermal damage variable. The following equation for the secant stiffness tensor is proposed [19,20],

$$C^s_{ijkl} = (1-d)C^h_{ijkl}(\omega) = (1-d)\left\{\frac{E(\omega)\nu(\omega)}{[1+\nu(\omega)][1-2\nu(\omega)]}\delta_{ij}\delta_{kl} + \frac{E(\omega)}{2[1+\nu(\omega)]}(\delta_{ik}\delta_{jl}+\delta_{il}\delta_{jk})\right\} \quad (4)$$

where $E(\omega)$ and $\nu(\omega)$ are the elastic modulus and the Poisson coefficient affected by the thermal damage process that can be obtained from tests. β_{ij} is the thermo-elastic coupling tensor that represents the stress induced for unit of temperature increase by the restricted thermal dilatation and can be expressed as follows,

$$\beta_{ij}(d,\omega) = -\frac{\partial^2\Psi}{\partial\theta\,\partial\varepsilon^e_{ij}} = C^s_{ijkl}(d,\omega)\alpha_{kl} \quad (5)$$

α_{kl} represents the dilatation coefficients tensor that in the isotropic case can be written as follows, $\alpha_{kl} = \alpha\delta_{kl}$. c_k is the specific heat or quantity of heat required to increase the temperature in 1°C and can be obtained as follows,

$$c_k(d,\omega) = -\theta\frac{\partial^2\Psi}{\partial\theta^2} \quad (6)$$

The other plastic part of the free energy density can be written as,

$$\Psi^p(p_i,\omega) = \frac{1}{2}p_i K_{ij}(\omega)p_j \quad (7)$$

where $K_{ij}(\omega)$ is plastic hardening tensor that depends on the thermal damage.

The total dissipation per unit of volume can be written as follows,

$$\Xi = \sigma_{ij}\dot{\varepsilon}_{ij} - \eta\dot{\theta} - \dot{\Psi} - \frac{1}{\theta}q_i\frac{\partial\theta}{\partial x_i} \geq 0 \quad (8)$$

where σ_{ij} is the stress tensor, ε_{ij} is the strain tensor, η the specific entropy, q_i is the heat conduction flux and x_i are the spatial coordinates.

The fulfilment of Clausius Duhem inequality is guaranteed if,

$$\sigma_{ij} = \frac{\partial\Psi^e}{\partial\varepsilon^e_{ij}} \quad (9)$$

$$\sigma_{ij} = C^s_{ijkl}(d,\omega)\varepsilon^e_{kl} - (\theta-\theta_o)\beta_{ij} \quad (10)$$

and the mechanical and thermal dissipation are both non negative,

$$\Xi_{qm} = \sigma_{ij}\dot{\varepsilon}^p_{ij} - \frac{\partial\Psi^{qp}}{\partial p_i}\dot{p}_i - \frac{\partial\Psi^e}{\partial d}\dot{d} - \frac{\partial\Psi}{\partial\omega}\dot{\omega} \geq 0 \quad (11)$$

$$\Xi_\theta = -\frac{1}{\theta}q_i\frac{\partial\theta}{\partial x_i} \geq 0 \quad (12)$$

The heat conservation equation can be obtained combining the First and Second Law of the Thermodynamics [18,6]. Assuming Fourier law for heat conduction, it results,

$$c_k\dot{\theta} - k\nabla^2_x\theta - l\dot{\omega} + (\theta\beta_{ij}\dot{\varepsilon}^e_{ij} - j\dot{d} - \Xi_{qm}) = r \quad (13)$$

where the term inside the brackets represents the thermo-mechanical coupling.

$$l = \frac{\partial^2\Psi}{\partial\omega\partial\theta} \quad (14)$$

$$j = \frac{\partial^2\Psi}{\partial d\partial\theta} \quad (15)$$

l is the latent heat of thermal damage ($l \leq 0$), k is the conductivity and $r$are the heat sources distributed per unit of volume.

2.2. Plastic process

The plastic threshold is defined by a yielding function that depends on the thermal damage [6,15,19],

$$F^p(\sigma_{ij},\kappa^p,\omega) = f^p(\sigma_{ij}) - K^p(\kappa^p,\omega) = 0 \quad (16)$$

where $K^p(\kappa^p,\omega)$ is the function of plastic hardening that depends on the thermal damage and on the plastic hardening variable κ^p [15].

Plastic strains are obtained from a plastic flaw rule,

$$\dot{\varepsilon}^p_{ij} = \dot{\lambda}\frac{\partial G}{\partial\sigma_{ij}} \quad (17)$$

where G is the plastic potential function and $\dot{\lambda}$ is the plastic consistence parameter. Eq. (16) can also be written as [21,19,20],

$$F^p(\sigma_{ij},\kappa^p,\omega) = f^p(\sigma_{ij}) - f^p_{red}(\omega)\bar{K}^p(\kappa^p) = 0 \quad (18)$$

$$\frac{f^p(\sigma_{ij})}{f^p_{red}(\omega)} - \bar{K}^p(\kappa^p) = 0 \quad (19)$$

$$\bar{F}^p(\sigma_{ij},\kappa^p,\omega) = \bar{f}^p(\sigma_{ij},\omega) - \bar{K}^p(\kappa^p) = 0 \quad (20)$$

where $0 \le f^p_{red} \le 1$ is a plastic reduction function due to the thermal damage process.

2.3. Mechanical damage process

The mechanical damage threshold is described through a damage function that is similar to the yield function of classical plasticity theory and also depends on the thermal damage variable [19,20],

$$F^d(\sigma_{ij},\kappa^d,\omega) = f^d(\sigma_{ij}) - K^d(\kappa^d,\omega) = 0 \quad (21)$$

where $K^d(\kappa^d,\omega)$ is the damage hardening function that depends on the thermal damage and the mechanical damage hardening variable κ^d, which is a normalized measure of the energy dissipated by mechanical damage [15].

Eq. (21) can also be written as,

$$f^d(\sigma_{ij}) - f^d_{red}(\omega)\bar{K}^d(\kappa^d) = 0 \quad (22)$$

$$\frac{f^d(\sigma_{ij})}{f^d_{red}(\omega)} - \bar{K}^d(\kappa^d) = 0 \quad (23)$$

$$\bar{F}^d(\sigma_{ij},\kappa^d,\omega) = \bar{f}^d(\sigma_{ij},\omega) - \bar{K}^d(\kappa^d) = 0 \quad (24)$$

where $0 \le f^d_{red} \le 1$ is a damage reduction function due to the thermal damage process.

3. Damage and plastic loading/unloading conditions

Damage and plastic loading/unloading conditions are given by a generalization of Kuhn Tucker conditions and can be written as follows [15],

$$\begin{cases} a)\ \dot{\lambda} \ge 0 \\ b)\ \bar{F}^p \le 0 \\ c)\ \dot{\lambda}\bar{F}^p = 0 \end{cases} \quad \begin{cases} a)\ \dot{d} \ge 0 \\ b)\ F^d \le 0 \\ c)\ \dot{d}F^d = 0 \end{cases} \quad (25)$$

3.1. Thermal damage evolution

In the same way as for the case of mechanical damage and plasticity, a complementary law must be formulated in order to describe the process of thermal damage. According to the thermodynamics, this law must be written in terms of the thermodynamic force associated to thermal damage and this requires the explicit formulation of the third term of free energy Ψ^ω.

Alternatively, the thermal damage evolution can be indirectly obtained [6]. In the solution of the thermal damage problem it is assumed that the characteristic time of this process can be neglected if compared with the characteristic time of the heat conduction in concrete structures so that the thermal damage can be expressed as a function of the maximum attained temperature [6]. To define this function the effects in the elastic modulus are used because it is the most sensible to the effects of high temperatures mechanical property. Assuming that the relation between the reduction of the elastic modulus and the initial one is proportional to the thermal damage variable, experimental curves relating the elastic modulus with temperature can be used to express this function as,

$$\omega(\theta) = 1 - \frac{E(\theta)}{E_o} \quad (26)$$

3.2. Numerical solution of the coupled thermo-mechanical problem

When the problem of concrete elements exposed to high temperatures is analysed, there exist three problems that interact each on the other: the thermal problem, the mechanical problem and the thermal damage problem.

Temperature produces thermal damage and influences the mechanical problem, since its variations produce thermal strains and stresses if the strains are restricted.

On the other hand, elastic, plastic and damage properties that take part in the mechanical analysis evolve with the thermal damage process.

A heat reduction that alters the thermal history of concrete also results from the thermal damage process.

All the other coupling effects are neglected in this paper.

Taking into account that the thermo-mechanical coupling and the thermal damage-mechanical coupling are predominant in the direction previously indicated, an incrementally uncoupled solution technique is proposed. For each time increment, the thermal and thermal damage problems are simultaneously solved and, then, assuming the temperature and thermal damage field obtained constant, the mechanical problem is solved.

When a concrete structure is subjected to high temperatures very high stress are generated if there exists any type of deformation constrain. As a result, the mechanical problem becomes strongly non-linear and in most cases, a time-sub-incrementation is required to solve this part of the problem [23].

The uncoupled equilibrium equation can be obtained by conventional finite element procedures and result,

$$\begin{cases} \boldsymbol{M}_{\mathbf{u}}\ddot{\boldsymbol{U}} + \boldsymbol{f}^{\mathbf{int}}_{\mathbf{u}} - \boldsymbol{f}^{\mathbf{ext}}_{\mathbf{u}} = \boldsymbol{0} \\ \boldsymbol{C}_\theta\dot{\Theta} + \boldsymbol{K}_\theta\Theta - \boldsymbol{f}_\theta - \boldsymbol{f}_\omega = \boldsymbol{0} \end{cases} \quad (27,28)$$

where $\boldsymbol{U}$ is the nodal displacements vector, Θ is the nodal temperatures vector, $\boldsymbol{M}_u$ is the dynamic mass matrix, $\boldsymbol{f}^{\mathbf{int}}_{\mathbf{u}}$ is the internal forces vector, $\boldsymbol{f}^{\mathbf{ext}}_{\mathbf{u}}$ is the external mechanical forces vector, $\boldsymbol{C}_\theta$ is the caloric capacity matrix, $\boldsymbol{K}_\Theta$ is the thermal conductivity matrix, $\boldsymbol{f}_\theta$ is the thermal forces vector and $\boldsymbol{f}_\omega$ is a vector related to the heat loss due to the thermal damage [6].

$$\boldsymbol{M}_{\mathbf{u}} = \int \boldsymbol{N}_{\mathbf{u}}^{\mathbf{T}} \rho \boldsymbol{N}_{\mathbf{u}} dV \tag{29}$$

$$\boldsymbol{f}_{\mathbf{u}}^{\mathbf{int}} = \int \boldsymbol{B}^{\mathbf{T}} \sigma dV \tag{30}$$

$$\boldsymbol{f}_{\mathbf{u}}^{\mathbf{ext}} = \int \boldsymbol{N}_{\mathbf{u}}^{\mathbf{T}} \boldsymbol{b} dV + \oint \boldsymbol{N}_{\mathbf{u}}^{\mathbf{T}} \mathbf{t}\, dS \tag{31}$$

$$\boldsymbol{C}_{\theta} = \int \boldsymbol{N}_{\theta}^{\mathbf{T}} c_k \boldsymbol{N}_{\theta} dV \tag{32}$$

$$\boldsymbol{K}_{\boldsymbol{\theta}} = \int [(\nabla \boldsymbol{N}_{\boldsymbol{\theta}})^T k (\nabla \boldsymbol{N}_{\theta})] dV + \oint \boldsymbol{N}_{\theta}^T h \boldsymbol{N}_{\theta} dA \tag{33}$$

$$\boldsymbol{f}_{\boldsymbol{\theta}} = \int \boldsymbol{N}_{\boldsymbol{\theta}}^{\mathbf{T}} r dV - \oint \boldsymbol{N}_{\boldsymbol{\theta}}^{\mathbf{T}} \mathbf{q} dA - \oint \boldsymbol{N}_{\theta}^T h \theta_{ext} dA \tag{34}$$

$$\boldsymbol{f}_{\omega} = \int \boldsymbol{N}_{\theta}^{\mathbf{T}} l \dot{\omega} dV \tag{35}$$

where $\boldsymbol{N}_{\mathbf{u}}$ are the displacement interpolation functions, ρ is the density, $\boldsymbol{N}_{\theta}$ are the temperature interpolation functions, $\boldsymbol{B}$ is the matrix relating the strains with the nodal displacements, $\boldsymbol{b}$ is the volumetric external forces vector, $\boldsymbol{t}$ is the external surface forces vector, c_k is the specific heat per unit of volume, k the thermal conductivity, h is the conduction convection coefficient (or surface coefficient) and $\boldsymbol{q}$ is the heat flux per unit area.

The resulting thermal problem described by Eq. (28) is similar to a conventional thermal problem with an augmented specific heat. Eq. (28) is solved with an Euler–Backward scheme that is unconditionally stable. The time step if then conveniently subdivided in n sub increments of time for which eq. (27) is solved with Newmark's method.

For the proposed constitutive model, yielding and damage equations must be integrated simultaneously. An Euler-Backward algorithm [15] is used for this purpose.

Between two equilibrium configurations n and $n-1$ the variables of the problem are updated as follows:

$$(\varepsilon_{ij}^p)_n = (\varepsilon_{ij}^p)_{n-1} + \Delta\lambda \left(\frac{\partial G}{\partial \sigma_{ij}}\right)_n \tag{36}$$

$$(\alpha_i)_n = (\alpha_i)_{n-1} + \Delta\lambda (H_i)_n \tag{37}$$

$$d_n = d_{n-1} + \Delta d_n \tag{38}$$

$$(\sigma_{ij})_n = (1-d_n) C_{ijkl}^o [(\varepsilon_{kl})_n - (\varepsilon_{kl}^p)_n] \tag{39}$$

Replacing these equations in the yielding and damage conditions described by Equations (20) and (24), the following non-linear system of equations is obtained:

$$\begin{cases} H^p(\Delta\lambda_n, \Delta d_n) = \bar{F}^p[(\sigma_{ij})_n, (\kappa^p)_n; \omega_n] = 0 \\ H^d(\Delta\lambda_n, \Delta d_n) = \bar{F}^d\,[(\sigma_{ij})_n, (\kappa^d)_n; \omega_n] = 0 \end{cases} \tag{40}$$

This system can be solved, for example, by the Newton Raphson method:

$$\begin{Bmatrix} \Delta\lambda_n^k \\ \Delta d_n^k \end{Bmatrix} = \begin{Bmatrix} \Delta\lambda_n^{k-1} \\ \Delta d_n^{k-1} \end{Bmatrix} - \begin{bmatrix} \left(\frac{\partial H^p}{\partial \Delta\lambda}\right)_n^{k-1} & \left(\frac{\partial H^p}{\partial \Delta d}\right)_n^{k-1} \\ \left(\frac{\partial H^d}{\partial \Delta\lambda}\right)_n^{k-1} & \left(\frac{\partial H^d}{\partial \Delta d}\right)_n^{k-1} \end{bmatrix}^{-1} \begin{Bmatrix} H^p(\Delta\lambda_n^{k-1}, \Delta d_n^{k-1}) \\ H^d(\Delta\lambda_n^{k-1}, \Delta d_n^{k-1}) \end{Bmatrix} \tag{41}$$

4. Application examples

4.1. Residual strength tests

The proposed model was calibrated [19,20,24] with the values of the residual mechanical properties obtained in the tests performed in LEMIT [3,13]. Additionally, the thermal and mechanical tests where numerically simulated in order to compare the results with experimental ones and to validate the model.

First, cylindrical specimens of (150 × 300 mm) were exposed to different maximum temperatures and cooling regimes [3,13]. One group of specimens identified as 'control' was left as reference of the behaviour at ambient conditions. The rest of the specimens were subjected to different maximum temperatures, from 150°C to 700°C. An electric furnace with automatic temperature control was used for the heating of the specimens. The heating rate, measured with thermocouples inserted in the concrete, was about 100°C/h. The maximum temperature was kept constant during an hour. Then, the specimens were subjected to two different types of cooling regimens. One group was left in the furnace for a slowly cooling and the other was rapidly cooled with spurts of cold water during half an hour. The specimens are identified with the maximum temperature attained (150, 300, 500, 700°C) followed by the type of cooling regime (a, air; w, water).

After the thermal treatment, all the specimens were tested under uniaxial compression.

Additionally, a group of prismatic specimens was subjected first to the thermal treatment and then tested under flexure in order to determine the residual facture energy.

The average values obtained from three tests, for the residual elastic modulus, Poisson coefficient, compression strength, tension strength and fracture energy for different maximum temperatures and cooling regimes are presented in Table 1.

The elasticity modulus and the Poisson coefficient were evaluated for a stress level corresponding to 40% of the compression strength.

The strength losses are greater when the specimens are rapidly cooled than when they are slowly cooled.

Table 1
Residual mechanical properties

Test	Elastic Modulus E [MPa]	Poisson's ratio ν	Compres. elastic limit f_{cy} [MPa]	Compres. strength f_c [MPa]	Tension strength f_t [MPa]	Fracture energy G_f [N/m]
Control	34961	0.169	30.5	39.3	6.1	255
150 a	32427	0.18	25	38.6	5	219
300 a	22982	0.12	17	28.2	3.4	175
500 a	14445	0.09	10	23.3	2	135
300 w	22773	0.09	20	27.7	4	-----
500 w	13594	0.035	10	22.4	2	200
700 w	5055	0.03	4	16.4	0.8	140

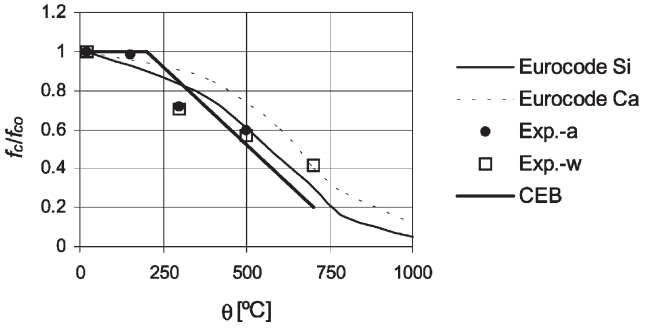

Fig. 1. Strength variation with maximum exposure temperature.

This effect is due to the fact that, in addition to degradation produced by the elevated temperatures, the rapid cooling produces a thermal shock that is not compensated by the possible re-hydratation of the cement paste in contact with water. The effect of the type of cooling regime in the elastic modulus is not so marked.

The values of strength loss and stiffness degradation obtained are compared with those in CEB and Eurocode [12] in Figs. 1 and 2. It can be observed the results obtained in LEMIT follow the general tendency of the curves presented in the mentioned codes.

First, the thermal part of the tests was simulated in order to prove the thermal model and to verify that a uniform temperature and resulting uniform thermal damage was attained inside the specimens during the heating process.

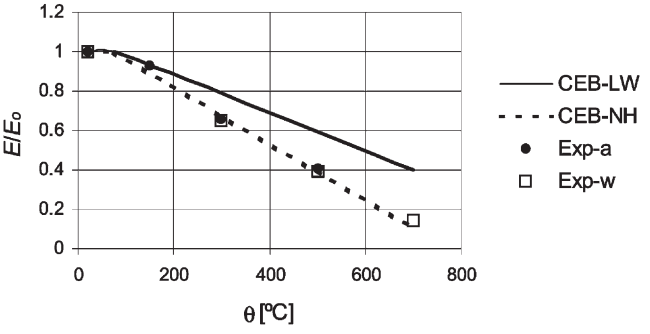

Fig. 2. Elastic modulus with maximum exposure temperature.

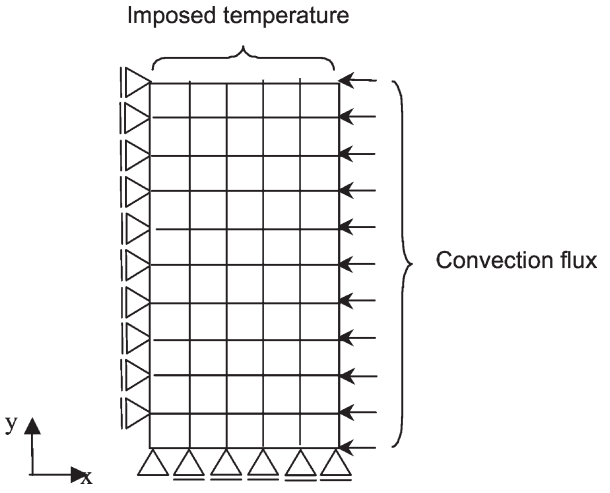

Fig. 3. Finite element mesh.

A quarter of the cylindrical specimen was modelled with the finite element mesh and thermal and mechanical boundary conditions illustrated in Fig. 3. The finite element mesh consists of 50 four-node elements with two integration points in each direction. The thermal properties used for concrete are presented in Table 2. The furnace temperature was imposed on the upper face of the model and convection flux was assumed in the lateral surface. The reference temperature was taken as 20°C.

The evolution of the furnace temperature and that obtained in the centre of a specimen exposed to a maximum temperature of 500°C and their comparison with experimental values are presented in Fig. 4. It can be observed that the temperature obtained in the centre of the specimen is always less than that experimentally

Table 2
Thermal properties of concrete

Conductivity coefficient: k = 2.5 J/(s m °C)
Conduc–convec coefficient: h = 4.6 J/(s m^2 °C)
Specific heat: c_k = 1041 J/(°C kg)
Thermal dilation coefficient: $\alpha = 10^{-5}$/°C

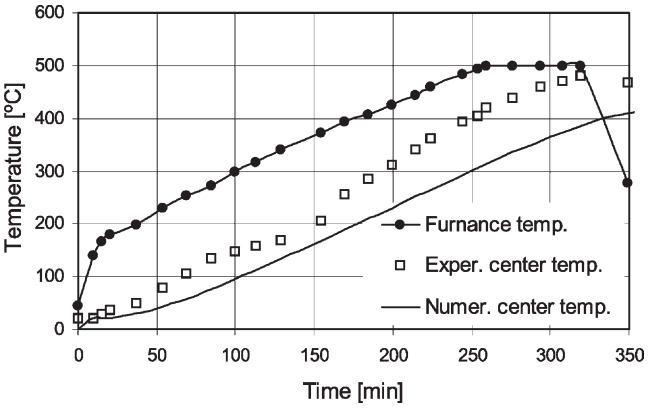

Fig. 4. Temperature time history.

registered. The difference can be attributed to the fact that the furnace heating was probably not perfectly uniform like in the numerical simulation and, additionally, the thermocouple inserted in the concrete could have produced certain disturbance of the temperature field. In spite of this observation, the temperature inside the specimen almost attained that of the furnace and the consequently thermal damage resulted almost uniform inside the specimen. Fig. 5 shows the temperature distribution for different times during the heating and cooling regimes of the specimen. It is clear that at the end of the heating process (t=330 min) temperature is almost uniform inside the specimen.

Based on the preceding observation and taking into account the variation of the elastic modulus with temperature indicated in Table 1, the model was calibrated [19]. Fig. 6 shows the variation of the thermal damage with temperature obtained with Eq. (26). It should be noted that the curves of thermal damage defined for the different types of cooling regime are practically coincident. For this model, the thermal damage variation

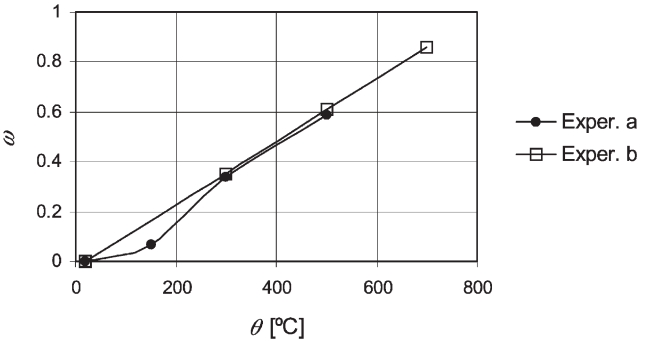

Fig. 6. Variation of thermal damage with maximum exposure temperature.

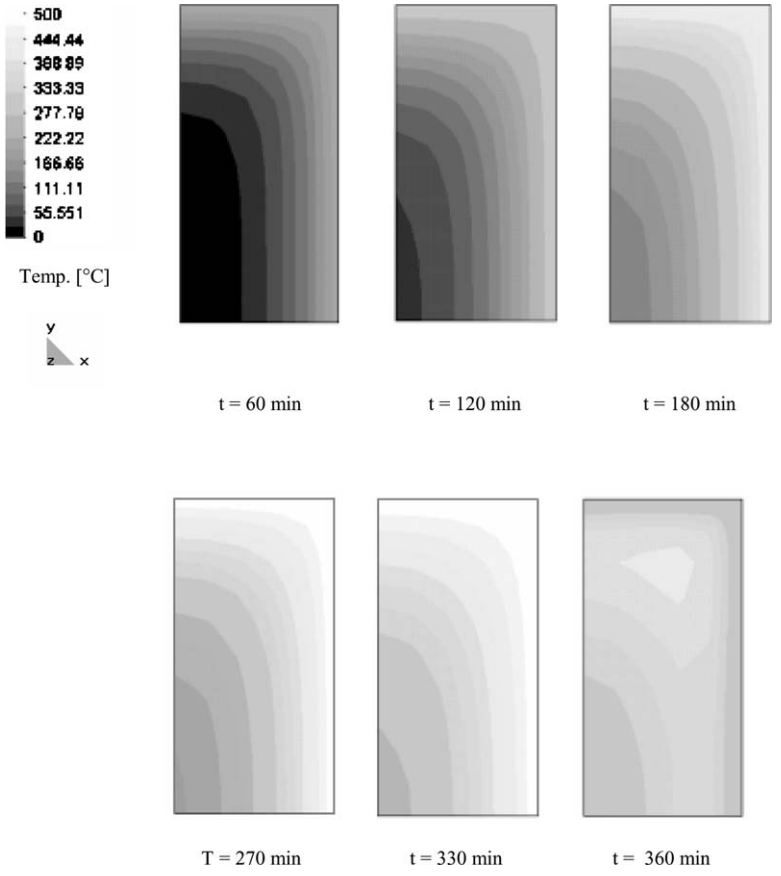

Fig. 5. Temperature field for different time instants.

defined from the elastic modulus is a measure of the global deterioration produced by high temperatures and simultaneously includes many effects in addition to the dehydratation process mentioned by Ulm [6]. It should be noted that when the specimen is cooled, temperature gradually returns to ambient temperature but thermal damage remains as an irreversible measure of the deterioration produced by high temperatures.

Combining Fig. 6 with Table 1, the variations of elastic modulus, Poisson coefficient, compression strength and fracture energy with thermal damage plotted in Fig. 7 are obtained.

The experimental and numerical stress–strain curves for the residual compression tests are presented in Fig. 8. Experimental and numerical strains are referred to that corresponding to stress level of 5 MPa to discard initial experimental effects in the supports. A good agreement between numerical and experimental results is achieved. Not only the maximum strength, but also all the deformation response of the specimens, both in axial and transversal directions, is reproduced.

It can be observed in Fig. 8 that the control specimen presents a linear behaviour until 40% of the maximum strength and that the linear range decreases as a consequence of the exposure to high temperatures.

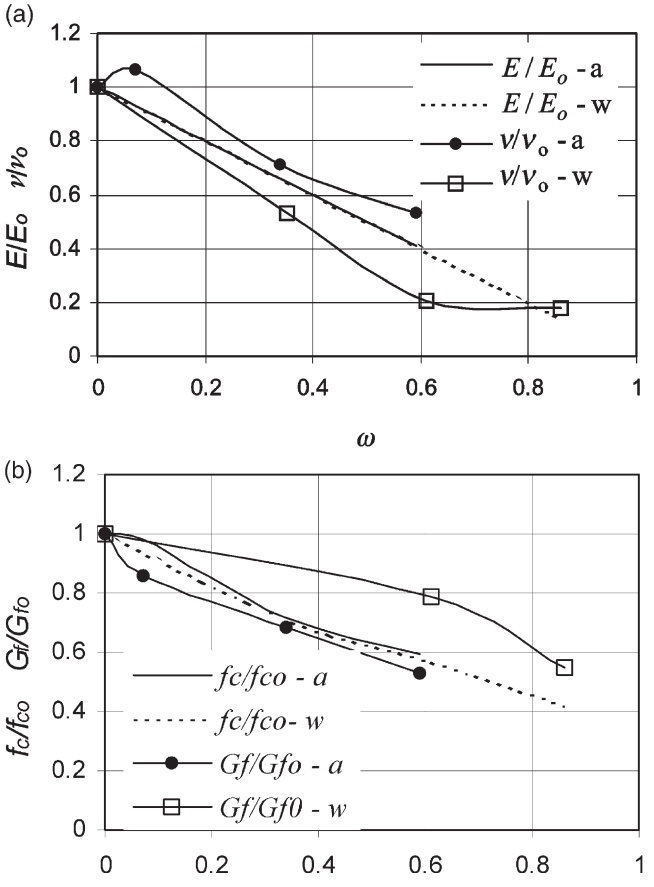

Fig. 7. Variation of mechanical properties with thermal damage. (a) Elastic modulus and Poisson coefficient; (b) Compression strength and fracture energy.

The dimensions and loading set up of the beams tested under flexure are shown in Fig. 9. This test was modelled as plane stress problem with the finite element mesh shown in Fig. 10. Triangular elements of three nodes and one integration point were used.

The load-vertical displacement of the central section curves numerically obtained and their comparison with experimental results are shown in Fig. 11. In general, a good agreement between numerical and experimental results is achieved.

If the post-pick regime is analysed in Fig. 11 it can be noted that the control beam presents a steeper softening than those exposed to high temperatures for which the softening is not so marked due to the ramification of cracks.

Comparing Figs. 11b and 11c it can be observed that for the same maximum temperature, the curve corresponding to the rapid cooling presents more curvature than that corresponding to the beam slowly cooled. This fact, that reflects the damage produced by the thermal shock is reproduced with the model, although it is not explicitly taken into account in the formulation.

As illustration example, the stress–strain curves corresponding to cyclic uniaxial compression tests of concrete specimens previously subjected to different levels of temperature are presented in Fig. 12. The mechanical properties of concrete at ambient temperature correspond to the cyclic tests performed by Sinha [25,15] and have been resumed in Table 3. The coupled effect of plasticity, mechanical damage and thermal damage is evident in this Figure.

4.2. Fire in the English Channel Tunnel [26]

The numerical simulation of the fire that produced serious damage in the Channel Tunnel in 1996 is presented in this section.

The finite element mesh for the concrete wall and the surrounding rock and the boundary conditions used are presented in Fig. 13. 300 plane strain elements of four nodes and four integration points were used. The mechanical and thermal properties of the materials are presented in Table 4.

Temperature was directly imposed in the superior quarter of the tunnel and convection flux was supposed in the rest of the surface. The temperature time history was assumed to have followed that prescribed in ISO 834 [12] [22] with a maximum temperature of 700°C and an initial temperature θ_0 of 20°,$\theta_{imp}(t) = \theta_0 + 345 \log_{10}(8t + 1) \leq \theta_{imp}^{max} = 700°C$

The distribution of temperatures and thermal damage after 12 h of fire is presented in Fig. 14. It can be observed that temperatures are not uniformly distributed and, as a result, there appear stresses that contribute to

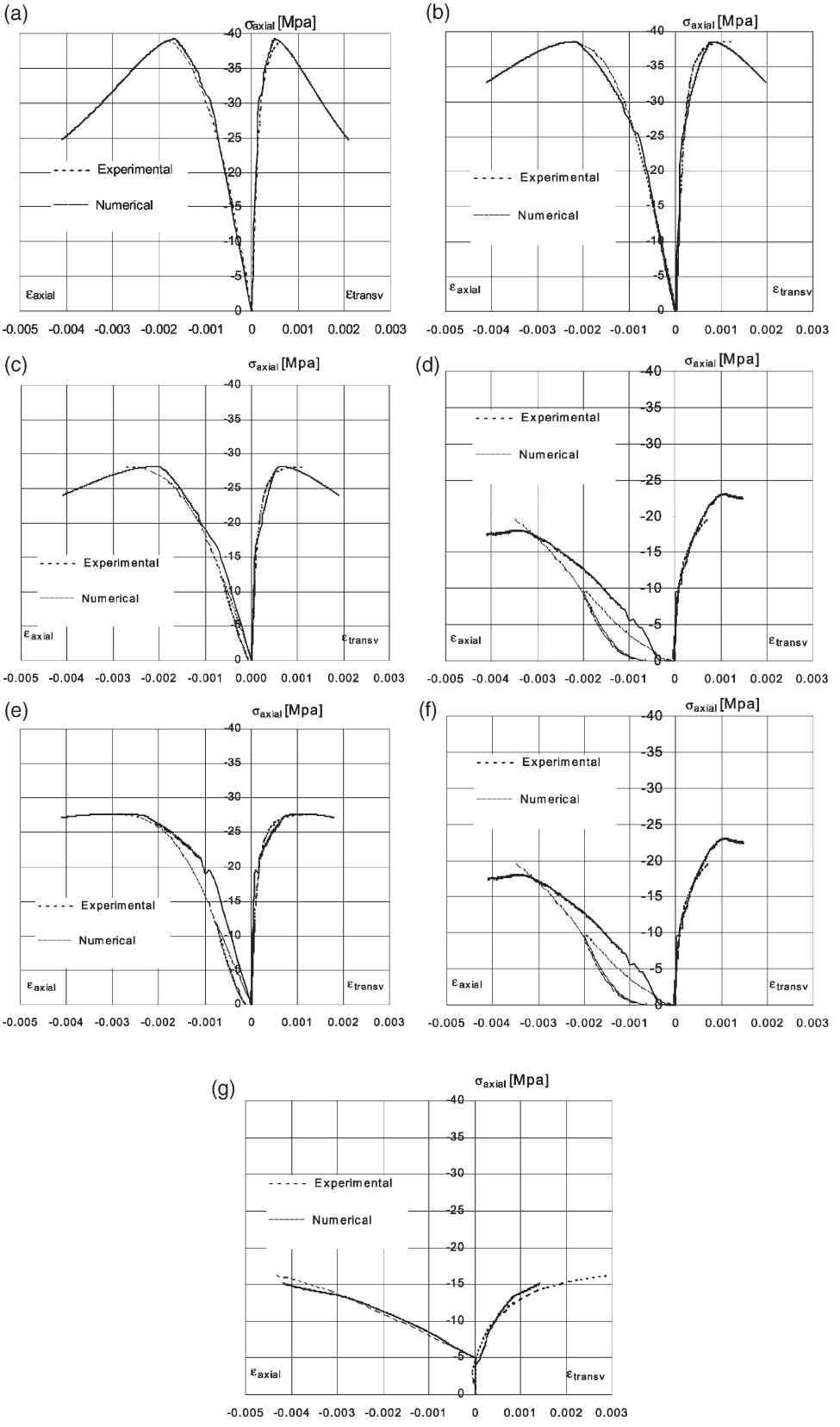

Fig. 8. Uniaxial residual compression tests. (a) Control, (b) 150a, (c) 300 a, (d) 500 a, (e) 300 w, (f) 500 w, (g) 700 w.

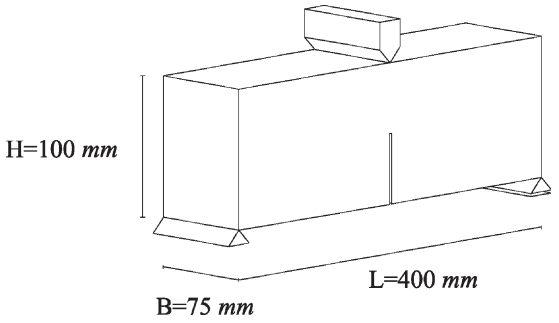

Fig. 9. Specimens tested under flexure.

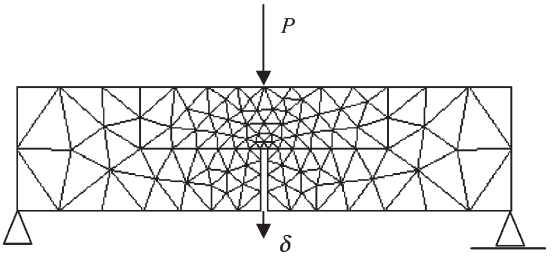

Fig. 10. Finite element mesh.

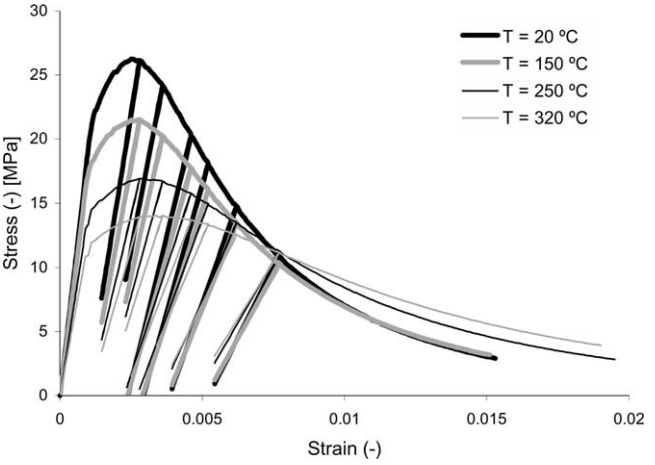

Fig. 12. Cyclic uniaxial compression tests for concrete previously subjected to different maximum temperatures.

the deterioration of concrete. Fig. 15 shows the distribution of resulting mechanical damage. It may be noted that mechanical damage is higher in the interior layers near to the surface of the wall than in the surface itself.

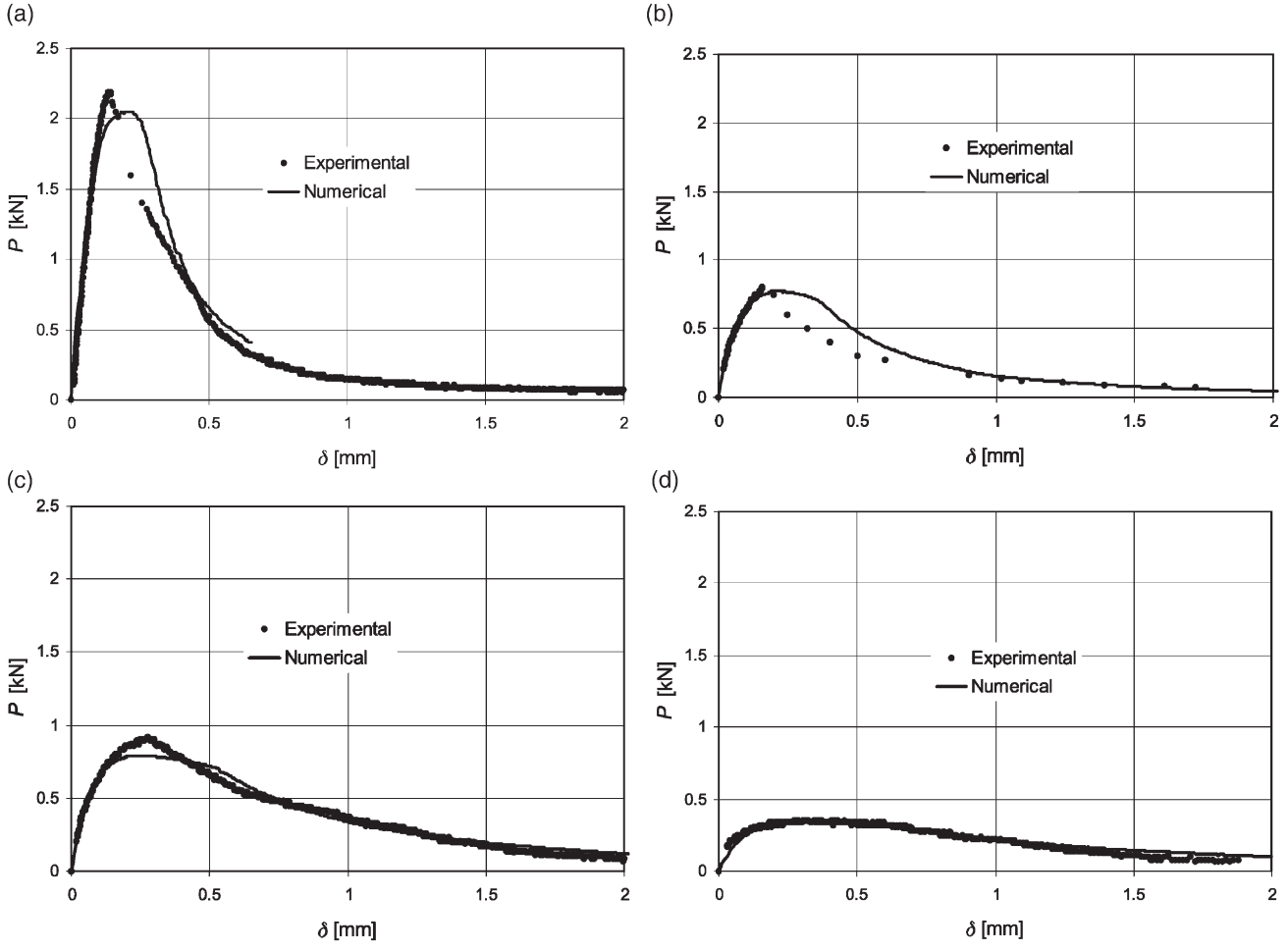

Fig. 11. Flexure tests. (a) Control, (b) 500 a, (c) 500 w, (d) 700 w.

Table 3
Mechanical properties of concrete (20°C)

E_o=19324.4 MPa
$\nu_o = 0.24$ Yielding criteria Lubliner–Oller [15] Associate flaw Damage criteria: Lubliner–Oller [15] $f_{cy}^{p} = 22.0$ MPa (Uniaxial compression plastic threshold) $f_{cy}^{d} = 20.0$ MPa (Uniaxial compression damage threshold) $f_{co} = 26.5$ MPa (Peak compression stress) $\frac{f_{co}}{f_{to}} = 10$ (Compression to tension strength ratio) $G_f^p = 80$ N/m; $G_c^p = 30000$ N/m; $G_f^d = 80$ N/m; $G_c^d = 10000$ N/m

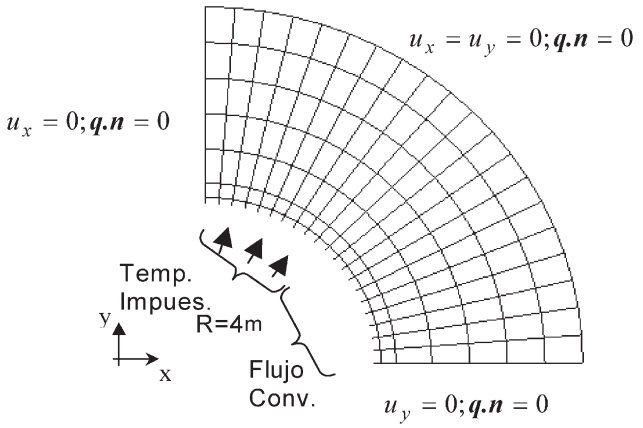

Fig. 13. Finite element mesh.

Table 4
Mechanical and thermal properties of concrete and rock

Property	Concrete	Rock
c_k[kJ/(m³°C)]	2500	2000
k[kJ/(h m°C)]	8	8
h[kJ/(h m²°C)]	15	—
E_o[GPa]	42	4
ν_o	0.2	0.25
f_{to}[MPa]	6.4	Elastic
f_{co}[MPa]	80	Elastic
α[1/°C]	10^{-5}	10^{-5}

This fact explains the spalling of concrete in the walls of the tunnel observed after the fire.

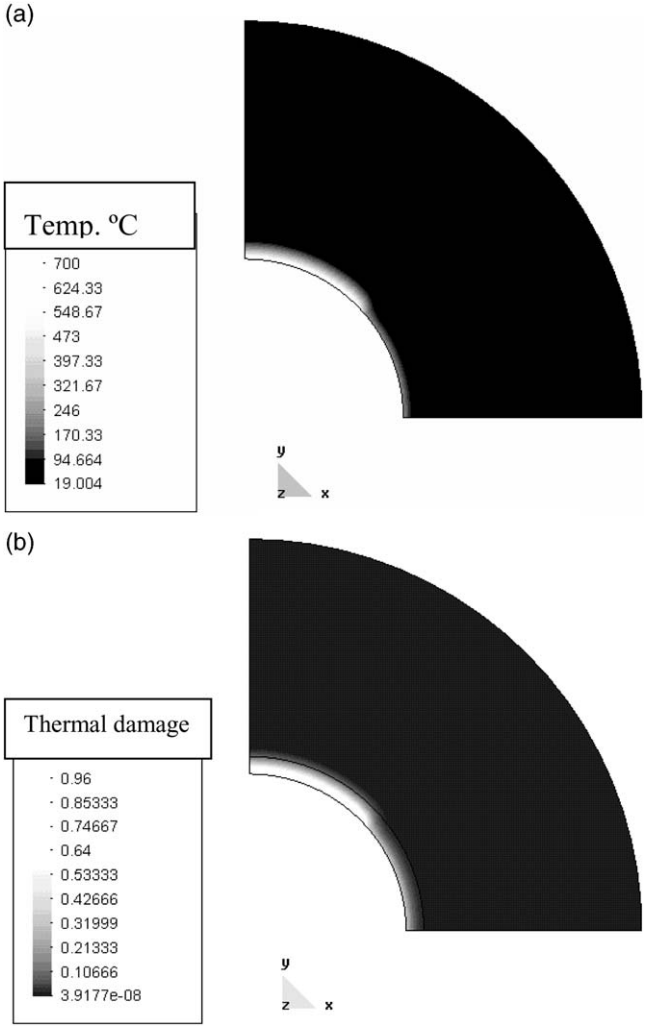

Fig. 14. Thermal variables after 12 h of fire. (a) Temperature field; (b) Thermal damage field.

5. Conclusions

A coupled plastic-damage model for the simulation of the thermo-mechanical behaviour of concrete simultaneously exposed to high temperatures and mechanical loads is presented in this paper. The model takes into account the effects of elevated temperatures through the thermal damage variable that is a measure of the deterioration due to temperature. The thermal damage variable represents the global damage resulting from the combi-

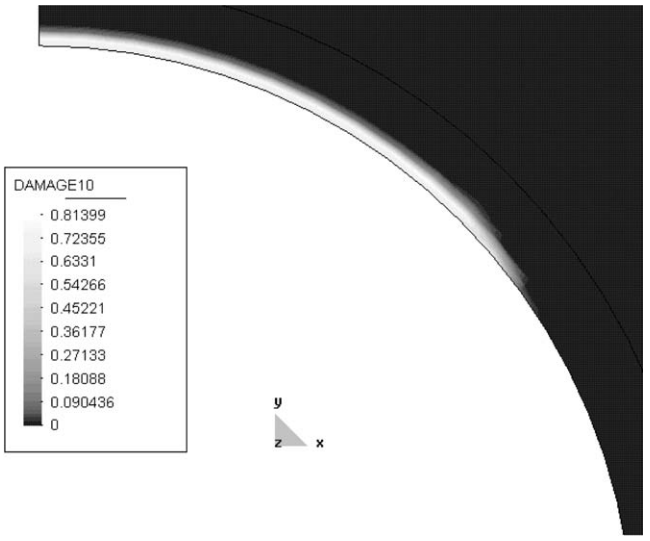

Fig. 15. Mechanical damage field.

nation of many complicated phenomena that take place in concrete as consequence of the exposure to high temperatures.

In line with the concept of the irreversibility of damage, the thermal damage variable is irreversible. This fact represents an advantage from other models that use temperature dependent functions.

The evolution law for the thermal damage variable can be indirectly obtained from experimental results. For this purpose, the variation of the elasticity modulus (the mechanical property most sensitive to elevated temperatures) is used.

In contrast to the scalar damage, frequently used for mechanical behaviour of concrete, the thermal damage produces isotropic stiffness degradation with reduction of both the elastic modulus and Poisson's ratio.

The thermal damage process affects all the inelastic behaviour of concrete.

Although the problem implies three coupled phenomena the numerical solution can be developed using a staggered technique with time sub-incrementation of the mechanical problem.

The application examples presented show that the model is able to simulate the residual mechanical behaviour of concrete exposed to high temperatures, characterized by the stiffness and strength loss, reduction of the Poisson's ratio and modification of the inelastic behaviour. Moreover, the complete coupled thermo-mechanical behaviour of structures exposed to high temperatures and simultaneously subjected to mechanical loads can be reproduced.

Acknowledgements

The financial support of CONICET and National University of Tucumán is gratefully acknowledged.

References

[1] Bazant ZP, Kaplan MF. Concrete at high temperatures: material properties and mathematical models. London: Longman Group Limited, 1996.
[2] Heinfling G, Reynouard JM, Merabet O, Duval CA. Thermo-elastic model for concrete at elevat temperatures including cracking and thermo- mechanical interaction strains. In: Comp. Plasticity, Fundamentals and Applications. Barcelona, España: CIMNE; 1997. p. 1493–8.
[3] Di Maio A, Giaccio G, Zerbino R. Relación entre el módulo de elasticidad estático y dinámico de hormigones expuestos d altas temperaturas. In: Memorias de CONPAT 99, Montevideo, Uruguay. 1999. p. 331–8.
[4] Zhang B, Bicanic N, Pearce CJ, Balabanic G. Residual fracture properties of normal and high-strength concrete subjected to elevated temperatures. Magazine of Concrete Research 2000;52(2):123–36.
[5] Ju JW, Zhang Y. Advanced thermomechanical constitutive models for airfield concrete pavement under high temperatures. In: Voyiadjis GZ, Ju JWW, Chaboche JL, editors. Damage mechanics in engineering materials. Elsevier; 1998. p. 275–83.
[6] Ulm FJ, Coussy O, Bazant Z. The Chunnel fire. I: chemoplastic softening in rapidly heated concrete. ASCE J. Eng. Mechs 1999;125(3):272–82.
[7] Huang Z, Burgess IW, Plank RJ. Non linear analysis of reinforced concrete slabs subjected to fire. ACI Structural Journal 1999;96(1):127–35.
[8] Huang Z, Burgess IW, Plank RJ. Three-dimensional analysis of composite steel-framed building in fire. ASCE J. Struc. Engng 2000;126(3):389–97.
[9] Huang Z, Burgess IW, Plank RJ. Effective stiffness modelling of composite concrete slabs in fire. Engineering Structures 2000;22:1133–44.
[10] Philleo R. Some physical properties of concrete at high temperatures. ACI Material Journal 1958;29(10):857–64.
[11] Lin WM, Lin TD, Powers-Couche LJ. Microstructures of fire-damaged concrete. ACI Material Journal 1996;93(3):199–203.
[12] Phan LT. Fire performance of high-strength concrete: a report of the state-of-the-art. <PDF/b96075.pdf> NISTIR 5934, 1996:115.
[13] Barragán B, Di Maio A, Giaccio G, Traversa L, Zerbino R. Efecto de las altas temeperaturas sobre las propiedades fisicomecánicas del hormigón. Ciencia y Tecnología del Hormigón, LEMIT, 1997;5:51–64.
[14] Gawin D, Mjorana CE, Pesavento F, Schrefler BA. A fully coupled multiphase model of hygro-thermo-mechanical behavior of concrete at high temperature. In: Computational Mechanics, New Trends and Applications. Barcelona, Spain: CIMNE; 1998. p. 1–19.
[15] Luccioni B, Oller S, Danes R. Coupled plastic-damaged model. Comp. Meths App. Mechs and Eng 1996;129:81–9.
[16] Lubliner J. Plasticity theory. USA: MacMillan Publishing, 1990.
[17] Stabler J, Baker G. On the form of free energy and specific heat in coupled thermo-elasticity with isotropic damage. Int. J. Solids and Structures 2000;37:4691–713.
[18] Maugin GA. The thermomechanics of plasticity and fracture. Cambridge: Cambridge University Press, 1992.
[19] Figueroa MI. Hormigones expuestos a altas temperatures. Master Thesis, National University of Tucumán, Argentina, 2001.
[20] Figueroa MI, Luccioni BM, Danesi RF. Modelo termo-mecánico para hormigón expuesto a altas temperatures. Mec. Comput 2001;XX:195–202.
[21] Salomón O, Oñate E, Oller S, Car E. Thermomechanical fatigue analysis based on continuum mechanics. Memorias de Mecom 99, Mendoza, Argentina 1999;133–142.
[22] Prato Grasso T. Comportamiento del hormigón en edades tem-

pranas. modelización y aplicaciones. PhD Thesis, UPC, Barcelona, España, 1999.
[23] Stabler J, Baker G. Fractional steps methods for thermo-mechanical damage analyses at transient elevated temperatures. Int. J. Num. Meths in Engineering 2000;48:761–85.
[24] Luege M, Luccioni B, Giaccio G, Zerbino R. Simulacion numérica del comportamiento de hormigones previamente expuestos a altas temperaturas. Mec. Comp 2000;XIX:157–62.
[25] Sinha BP, Gerstle KH, Tulin LG. Stress–strain relations for concrete under cyclic loading. ACI Structural Journal 1964;62(2):195–210.
[26] Ulm FJ, Acker P, Lévy M. The Chunnel fire. 2: Analysis of concrete damage. ASCE J. Eng. Mechs 1999;125(3):283–9.